J. Fluid Mech. (1991), *vol.* 223, *pp.* 325–355
Printed in Great Britain

The dissipative structure of shock waves in dense gases

By M. S. CRAMER AND A. B. CRICKENBERGER
Department of Engineering Science and Mechanics, Virginia Polytechnic Institute and State University, Blacksburg, VA 24061-0219, USA

(Received 17 April 1990)

The present study provides a detailed description of the dissipative structure of shock waves propagating in dense gases which have relatively large specific heats. The flows of interest are governed by the usual Navier–Stokes equations supplemented by realistic equations of state and realistic models for the density dependence of the viscosity and thermal conductivity. New results include the first computation of the structure of finite-amplitude expansion shocks and examples of shock waves in which the thickness increases, rather than decreases, with strength. A new phenomenon, referred to as impending shock splitting, is also reported.

1. Introduction

The most common representation of a shock wave is as a discontinuity propagating in an inviscid fluid. However, it is well known that the actual transition between the upstream and downstream states is continuous, the smoothing agent being a combination of heat transfer and viscous effects. A reasonable qualitative picture of the details of the flow within the shock layer is given by Taylor's (1910) structure for weak shocks propagating in perfect gases. More recent studies have shown that many of the features of compressible flow are contingent on the sign of the thermodynamic parameter

$$\Gamma \equiv \frac{1}{\rho}\frac{\partial(\rho a)}{\partial \rho}\bigg|_s = \frac{V^4}{2a}\frac{\partial^2 p}{\partial V^2}\bigg|_s. \tag{1.1}$$

Here ρ is the fluid density, $a = a(\rho, s)$ is the thermodynamic sound speed, s is the fluid entropy, $V \equiv \rho^{-1}$ is the specific volume, p is the thermodynamic pressure, and Γ is commonly referred to as the fundamental derivative of gasdynamics. In flows having $\Gamma < 0$, compression shocks violate the entropy inequality and the only shocks possible are expansion or rarefaction shocks; see e.g. Zel'dovich (1946) or the more recent discussion of Thompson (1971). We refer to this case as that of negative nonlinearity and that where $\Gamma > 0$ as positive nonlinearity.

The conditions under which Γ becomes negative were first given by Bethe (1942) and Zel'dovich (1946) who recognized that fluids with relatively large specific heats will possess a region of negative nonlinearity in the general vicinity of the saturated-vapour line at temperatures and pressures approaching the critical values. This region is depicted in figure 1 for the case of a van der Waals gas with a constant specific heat. This region of negative nonlinearity is necessarily bounded. After all, all gases behave like ideal gases in the limit of small density (large V). In the ideal-gas limit

$$\Gamma \to \frac{a}{\rho}\frac{\gamma+1}{2} > 0,$$

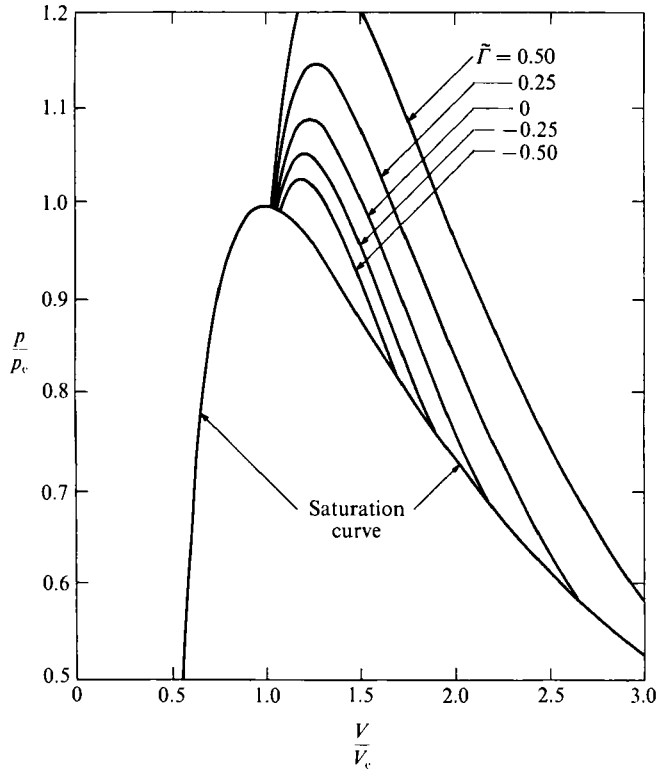

FIGURE 1. Constant $\tilde{\Gamma} \equiv \rho\Gamma/a$ contours for a van der Waals gas with $c_v = 50R$ = constant. The subscript c denotes conditions at the thermodynamic critical point.

where $\gamma > 1$ is the ratio of specific heats; thus, Γ must ultimately become positive as the density decreases. Lambrakis & Thompson (1972) and Thompson & Lambrakis (1973) have extended the work of Bethe and Zel'dovich by employing more sophisticated equations of state. Their work has provided examples of commercially available hydrocarbons and fluorocarbons which have a similar region of negative nonlinearity. In the following we shall refer to fluids that have a region of negative nonlinearity similar to that seen in figure 1 as Bethe–Zel'dovich–Thompson (BZT) fluids in recognition of the early contributions of these authors. Inspection of figure 1 shows that disturbances of sufficiently large amplitude may result in both positive and negative nonlinearity in the same disturbances i.e. Γ may change sign at various points in the flow field. Such cases are referred to as mixed nonlinearity and may result in phenomena not observed in either the $\Gamma > 0$ or the $\Gamma < 0$ theory. Examples include the formation and propagation of compression and expansion shocks in the same disturbance, collisions between expansion and compression shocks of the same family, the partial disintegration of both compression and expansion shocks into shock-fan combinations, the existence of sonic shocks and shock splitting. By sonic shocks we mean shocks having speed identically equal to the convected sound speed immediately before or after the shock. In a frame moving with a sonic shock the Mach number is unity on the sonic side of the shock. In steady flows, a sonic oblique shock has Mach lines parallel to the shock on the sonic side. Double sonic shocks are shocks that carry a non-zero pressure jump but that have sonic conditions on both sides of the shock. Details of these inviscid phenomena have been given by

Thompson & Lambrakis (1973), Cramer & Kluwick (1984), Cramer & Sen (1987), and Cramer (1989*a*); recent summaries have been provided by Cramer (1987*b*, 1989*c*). Previous investigations of the dissipative structure of shock waves in BZT fluids are, for the most part, based on the weak-shock theory of Cramer & Kluwick (1984) although the role of the structure in the context of the existence of finite-amplitude shocks has been delineated by Menikoff & Plohr (1989) and Cramer (1989*a*, *c*).

New features revealed by Cramer & Kluwick (1984) and Cramer (1987*a*) are as follows. (i) The density, temperature and pressure approach the inviscid conditions on the sonic side of a sonic shock algebraically rather than exponentially. (ii) The local Mach number has a maximum or minimum at points where the local value of Γ changes sign. (iii) All expansion shocks correspond to an entropy deficit. That is, $s(x) < s_1$, where s_1 is the entropy upstream of the shock, over most of the shock layer although the entropy difference ultimately becomes positive as the downstream conditions are approached.

Remarks similar to (i) have been made by Lee-Bapty & Crighton (1987) in their discussion of a cubic Burgers equation and by Cramer & Sen (1990) in the context of temperature shocks in superfluid helium. This slow algebraic approach tends to thicken the shock. When the sonic shock is the shock of maximum, rather than minimum, strength the thickening leads to an increase in thickness with strength as the sonic condition is approached. This contrasts sharply with the Taylor structure in which the thickness decreases monotonically with strength. Result (ii) also clearly contrasts with the perfect gas theory where Γ is strictly positive at every point in the flow. It is well known that the Mach number decreases monotonically from supersonic conditions to subsonic conditions if the gas is perfect. The significance of (iii) is seen when it is recalled that the local value of the entropy in a compression shock is always greater than the upstream value at every point in the shock layer. Thus, in a perfect gas, the entropy attains a local maximum, rather than minimum, at some point in the interior of a compression shock.

The principal goal of the present study is to provide detailed descriptions of the dissipative structure of finite-strength shocks in BZT fluids, thus extending and verifying the predictions of the Cramer–Kluwick weak-shock theory. We have also discovered a class of solutions which have no counterpart in either the weak-shock theory of Cramer & Kluwick (1984) or Taylor's (1910) classical theory. These solutions resemble an internal splitting of an admissible shock and reveal the physical mechanisms leading to the inviscid shock splitting described by Cramer (1989*a*) and Menikoff & Plohr (1989).

Our general approach is to consider single-phase Navier–Stokes fluids governed by the usual continuum shock structure model; this is described in the following section. *A posteriori* checks on the thickness, presented in §4, indicate that the continuum model is indeed justified. Realistic models are employed for the pressure, thermal conductivity and viscosities; these are described in §3. In order to provide a theoretical background for the new features revealed by our numerical calculations, we have presented an extension of the weak-shock theory of Cramer & Kluwick in §5. This theory is seen to be in reasonable qualitative agreement with all phenomena found in the numerical calculations.

2. Structure model and method of solution

The standard continuum model for the dissipative structure of a shock wave takes the flow to be one-dimensional, steady, single-phase, and free from all body forces.

Under these conditions, the Navier–Stokes–Fourier equations may be reduced to

$$\left.\begin{aligned} \frac{\mathrm{d}V}{\mathrm{d}x} &= F(V,T) \equiv \frac{p-p_1+m^2(V-V_1)}{m\mu\left(\frac{\mu_b}{\mu}+\frac{4}{3}\right)}, \\ \frac{\mathrm{d}T}{\mathrm{d}x} &= G(V,T) \equiv \frac{m}{k}\{e-e_1+[p_1-\tfrac{1}{2}m^2(V-V_1)](V-V_1)\}, \end{aligned}\right\} \tag{2.1}$$

where $V(\equiv\rho^{-1})$ and T are the specific volume and the absolute temperature. The functions $p = p(V,T)$, $e = e(V,T)$, $\mu = \mu(V,T)$, $k = k(V,T)$, $\mu_b = \mu_b(V,T)$ are the thermodynamic pressure, internal energy, shear viscosity, thermal conductivity, and bulk viscosity, respectively. The quantity

$$m = v\rho = v_1\rho_1 = v_2\rho_2 = \text{constant}, \tag{2.2}$$

where $v(x)$ is the local flow speed, is referred to as the mass flux. The subscripts 1 and 2 denote conditions on either side of the shock. Because $V = \rho^{-1}$, we may relate v to V through the mass flux m as follows:

$$v = \frac{m}{\rho} = mV.$$

The specific volume and temperature are required to approach constants as $x \to \pm\infty$, i.e.

$$\left.\begin{aligned} V, T &\to V_1, T_1 \quad \text{as} \quad x \to -\infty, \\ V, T &\to V_2, T_2 \quad \text{as} \quad x \to \infty. \end{aligned}\right\} \tag{2.3}$$

At the asymptotes (2.3), we have

$$F(V_i, T_i) = 0, \quad G(V_i, T_i) = 0, \tag{2.4}$$

where $i = 1, 2$. It can be verified that the combination of (2.2) and (2.4) are equivalent to the Rankine–Hugoniot conditions for a normal stationary shock in inviscid flow. With respect to solutions to the autonomous system (2.1), the solutions to (2.4) are seen to be singular points in the (T, V) phase plane; the desired solution is the integral of (2.1) which goes through the two singular points (V_1, T_1) and (V_2, T_2). Our approach to the solution to (2.1)–(2.3) is to recast the problem as an initial-value problem. In order to avoid the well-known numerical instabilities associated with the saddle point at the downstream asymptote, we begin the integration in the vicinity of this singular point. We choose the initial value of V to satisfy

$$V_{\text{init}} \approx V_2,$$

where V_{init} is our initial value of V. The initial temperature is then approximated by using the slope of the correct solution curve as follows:

$$T_{\text{init}} = T_2 + C(V_{\text{init}} - V_2),$$

$$C = \frac{G_T - F_V}{2F_T} - \left[\left(\frac{F_V - G_T}{2F_T}\right)^2 + \frac{F_T G_V - F_V G_T}{F_T^2}\right]^{\frac{1}{2}},$$

where F_T, F_V, G_T, G_V are the partial derivatives of F and G evaluated at condition 2. Even though small errors are introduced by this approximation, all solutions neighbouring the correct one enter the node at V_1, T_1 and a reasonably accurate solution is guaranteed.

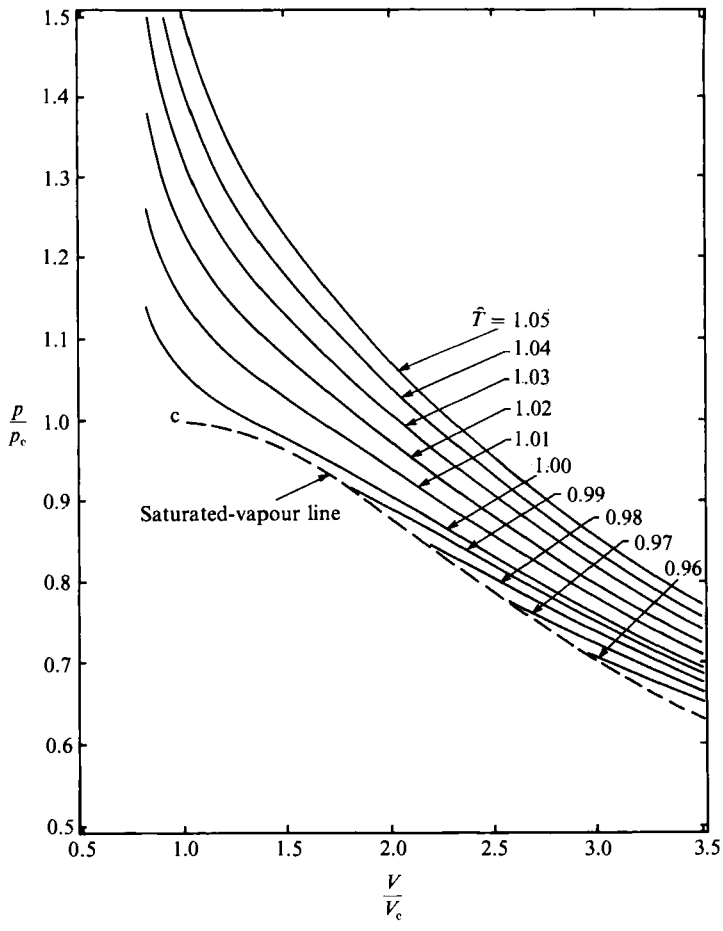

FIGURE 2. Shock adiabats for PP11. The adiabats for values of $\hat{T} < 1$ intersect the saturated vapour line at $T = \hat{T}T_c$. The adiabats for values of $T \geqslant 1$ go through the point $V = 1.35V_c$, $T = \hat{T}T_c$.

In the perfect-gas theory, all properties of a normal stationary shock can be determined by specifying the upstream conditions and, as a measure of strength, the upstream flow Mach number. Although it is rarely done, it is also possible to use a downstream thermodynamic variable to specify the strength. In our calculations, we use the latter and, in particular, the shock strength will be fixed by specifying the downstream value of the specific volume. The downstream temperature can then be computed by iterating the Hugoniot equation:

$$H(V_1, T_1, V_2, T_2) \equiv [e] + [V]\tfrac{1}{2}(p_2 + p_1) = 0, \tag{2.5}$$

which is recognized as the jump condition expressing the principle of energy conservation. Here square brackets denote the jump in the indicated quantity, i.e. $[A] \equiv A_2 - A_1$, where A is any quantity. Solutions to (2.5) plotted in the (p, V)-diagram are normally referred to as the shock adiabat. Shock adiabats for perfluoroperhydrophenanthrene, referred to hereinafter as by its trade name PP11, have been computed by this technique and are plotted in figure 2. Once T_2 is determined from (2.5), the downstream pressure and all other thermodynamic variables may be

determined through use of the equation of state. The upstream and downstream Mach numbers may then be determined by the well-known relation

$$m^2 = \left(\frac{M_2 a_2}{V_2}\right)^2 = \left(\frac{M_1 a_1}{V_1}\right)^2 = -\frac{[p]}{[V]}, \tag{2.6}$$

which is obtained by combining the mass and momentum jump conditions (2.2) and (2.4). Here $M \equiv v/a$ is the Mach number. It should also be noted that the mass equation (2.2) requires that

$$m = v\rho = \frac{Ma}{V} = \text{constant}.$$

Thus, from (2.6) we have the expression for the local Mach number at any point inside the shock layer:

$$M(x) = \frac{V}{a}\left(-\frac{[p]}{[V]}\right)^{\frac{1}{2}}.$$

To determine whether the shock is admissible we use the criterion given by Cramer (1989*a*) and Menikoff & Plohr (1989). This states that the shock is an admissible compression shock if and only if the Rayleigh line connecting the upstream and downstream states lies entirely above the shock adiabat between the upstream and downstream states. The term Rayleigh line refers to any straight line in the (p, V)-diagram. In like manner, the proposed discontinuity is an admissible expansion shock if and only if the Rayleigh line lies entirely below the adiabat. This existence condition is recognized as an extension of Lax's generalized entropy admissibility conditions, see e.g. Lax (1971). A similar result in the context of weak shocks with mixed nonlinearity has been given by Lee-Bapty & Crighton (1987).

3. Gas models

The equation of state used here can be written in general form as

$$p = \frac{RT}{V-b} + \sum_{i=1}^{N} Q_i F_i', \tag{3.1}$$

where R is the gas constant and b is a constant typically measuring the excluded volume. The functions $F_i(V)$ and $Q_i(T)$ will be specified later and a prime is used to denote differentiation with respect to the pertinent variables. The entropy and internal energy corresponding to (3.1) are

$$s = s_* + \psi + R\ln\left(\frac{V-b}{V_*-b}\right) + \sum_{i=1}^{N} (Q_i' F_i - Q_i'^* F_i^*),$$

$$e = e_* + \phi + \sum_{i=1}^{N} \{F_i(TQ_i') - F_i^*(T^*Q_i'^* - Q_i^*)\},$$

where

$$\psi \equiv \int_{T_*}^{T} \frac{c_{v\infty}}{T}\,\mathrm{d}T, \quad \phi = \int_{T_*}^{T} c_{v\infty}\,\mathrm{d}T,$$

where $c_{v\infty}$ is the ideal-gas specific heat, i.e.

$$c_{v\infty} = c_{v\infty}(T) \equiv \lim_{V\to\infty} c_v(V, T). \tag{3.2}$$

	Fluid	T_c (K)	p_c (atm)	Z_c	T_b (K)	ω	$\frac{c_{v\infty}(T_c)}{R}$	n
$C_{13}F_{22}$	pf-perhydrofluorene (PP10)	632	16.0	0.283	463	0.787	78.4	0.53
$C_{14}F_{24}$	pf-perhydrophenan threne (PP11)	650	14.4	0.269	488	0.777	97.3	0.58
$C_{18}F_{39}N$	pf-trihexylamine (FC-71)	646	9.3	0.275	526	0.97	145.0	0.43

TABLE 1. Fluids used in this study. Details of the estimation of the critical properties, boiling temperature and specific heat have been given by Cramer (1989*b*). In each case, the acentric factor ω was computed from the manufacturer's saturation data.

The asterisk subscript or supercript denotes a reference value which is usually evaluated at a specified temperature and a pressure of one atmosphere. In each case presented here we have taken T_* to be the critical temperature. The sound speed may be computed from

$$a(V,T) = V\left\{\frac{T}{c_v}(p_T)^2 - p_V\right\}^{\frac{1}{2}}, \tag{3.3}$$

where the actual specific heat is given by

$$c_v(V,T) = c_{v\infty}(T) - T\int_V^\infty p_{TT}\,\mathrm{d}V. \tag{3.4}$$

The subscripts T and V again denote partial derivatives which may be computed from (3.1) once the functions F_i and Q_i are specified. To compute the fundamental derivative from (3.1) we recast (1.1) in terms of p_T, p_V, p_{VV}, p_{VT}, p_{TT}, c_v, and $\partial c_v/\partial T$; the explicit form may be found in Bethe (1942), Lambrakis & Thompson (1972) or Cramer (1989*b*).

The equation of state chosen for the present calculations is that of Martin & Hou (1955) with the high-density correction found in the footnote on page 148 of that article. Thus, the functions F_i will comprise inverse integral powers of $V-b$ and the Q_i functions will be of the form

$$Q_i = q'_{i+1} + q''_{i+1}\,T + q'''_i \exp(-5.475T/T_c),$$

where q'_{i+1}, q''_{i+1}, q'''_{i+1} are constants computed as indicated in the article by Martin & Hou.

The Martin–Hou equation has a strong analytical basis and therefore requires a minimum number of input data. Furthermore, the work of Thompson & Lambrakis (1973) and Cramer (1989*b*) indicates that it is conservative with respect to predictions of negative nonlinearity. The required input parameters are the molecular weight, critical temperature, pressure and specific volume (T_c, p_c, V_c) and the normal boiling temperature (T_b).

The numerical values of p_c, T_c, and T_b for the fluids employed here are listed in table 1. The critical specific volume and molecular weight were used to compute the critical compressibility $Z_c \equiv p_c V_c/RT_c$. Most of the parameters shown were either taken directly from the manufacturer's information (ISC Chemicals Ltd., Bristol, England for PP10 and PP11 and 3M Corporation, Minneapolis, Minnesota for FC-71)

or estimated by standard techniques. Details of the estimation techniques are described by Cramer (1989*b*).

For a complete specification of the thermodynamic state we also require the ideal gas specific heat (3.2). For the present purposes it was adequate to model this by the power law

$$c_{v\infty} = c^*_{v\infty}\left(\frac{T}{T_*}\right)^n, \tag{3.5}$$

where n is a constant, $c^*_{v\infty}$ is the ideal gas specific heat evaluated at the reference temperature T_*. As in Cramer (1989*b*), both n and $c^*_{v\infty}$ were estimated by the group contribution method of Rihani & Doraiswany (1965).

The shear viscosity and thermal conductivity were computed by the method of Chung, Ajlan, Lee & Starling as described in Reid, Prausnitz & Poling (1987, chap. 9–10). Each fluid considered was regarded as non-polar so that the dipole moment and association factors were ignored. In addition to those already introduced the only other factor required for the application of these formulae is the eccentric factor

$$\omega \equiv -\log_{10}(p_s(T = 0.7T_c)/p_c) - 1,$$

where $p_s(T)$ is the saturation pressure. For the fluids listed in table 1, sufficient saturation data was provided in the manufacturer's product information to facilitate computation of ω.

Finally, the bulk viscosity must be specified. Data and analytic formulae for the bulk viscosity are scarce under the simplest conditions and are nonexistent for the heavy fluorocarbons considered in the present study. As a result, we have assumed that the ratio μ_b/μ is a constant. Again, owing to the lack of data, we choose numerical values for this ratio rather arbitrarily. However, several numerical tests and the analysis of §5 indicate that different choices will not make significant changes in the qualitative nature of the structure.

4. Results

In each of the cases described in this section, we have plotted scaled versions of the specific volume, entropy and the Mach number versus the scaled distance x/L. The lengthscale L is defined

$$L \equiv \mu_*\left(\frac{V_c}{p_c}\right)^{\frac{1}{2}}$$

where μ_* is the shear viscosity computed at the reference state. Thus, the length scaling is fixed for each fluid and no rescaling based on the shock strength is required. For purposes of comparison we have also shifted all profiles so that

$$x = 0 \quad \text{when} \quad V = \tfrac{1}{2}(V_1 + V_2).$$

The first example is a series of expansion shocks in PP10. The upstream state was taken to be

$$V_1 = 1.75V_c, \quad T_1 = 0.99T_c, \quad p_1 = 0.9194p_c, \quad \Gamma_1\rho_1/a_1 = -0.298.$$

At this temperature, the saturation pressure is estimated to be $0.924p_c$; thus, the upstream state is just to the right of the saturated-vapour curve in the (p, V)-diagram. The variations of the non-dimensional specific volume, entropy and Mach

$\frac{V_2}{V_c}$	$\frac{p_2}{p_c}$	$\frac{T_2}{T_c}$	$\frac{\Gamma_2\rho_2}{a_2}$	M_1	M_2	$\frac{s_2-s_1}{R}$ ($\times 10^5$)	$\frac{\tau}{L}$
1.95	0.8896	0.9876	−0.1633	1.014	0.989	0.72	1837
2.15	0.8589	0.9855	−0.0222	1.023	0.988	3.93	1289
2.35	0.8279	0.9836	0.1002	1.027	0.995	7.63	1360

TABLE 2. Numerical data for the expansion shocks of figures 3–5. Fluid is PP10 with $V_1 = 1.75V_c$, $T_1 = 0.99T_c$, $p_1 = 0.9194p_c$, $\rho_1\Gamma_1/a_1 = -0.298$, and $\mu_b/\mu = 0.5$.

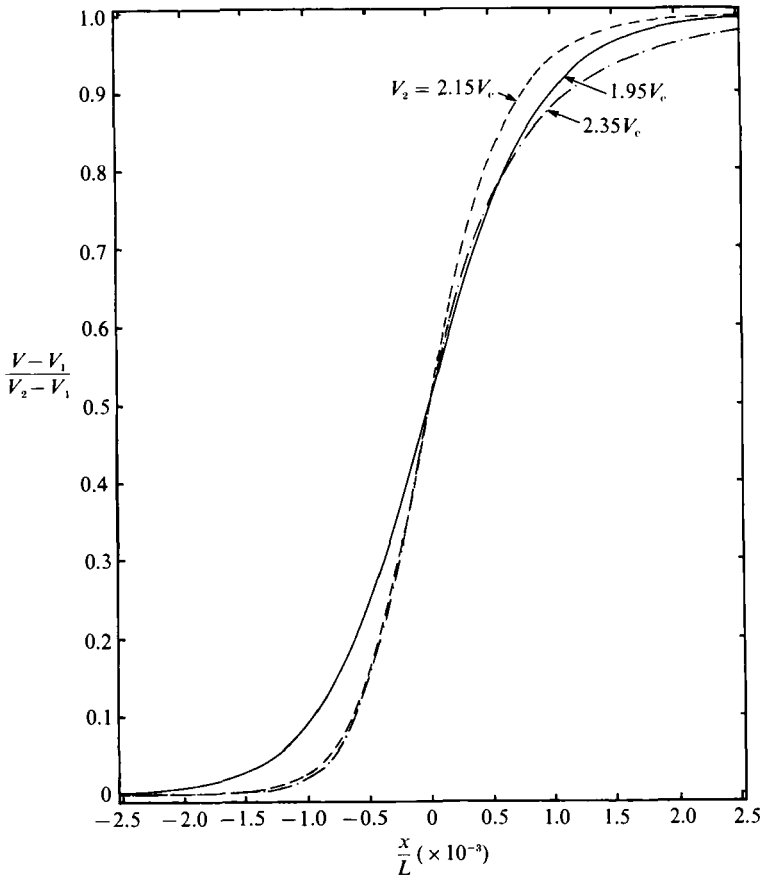

FIGURE 3. Variation of specific volume *vs.* x for three expansion shocks in PP10. Numerical data are given in table 2.

number through the shock layer are given in figures 3–5. The downstream conditions, Mach numbers and scaled thickness are listed in table 2. Throughout, we employ a shock thickness based on the standard maximum slope criterion; the dimensional thickness is denoted by τ. The non-dimensional variations of the entropy jump, Mach numbers and thickness for this fluid and upstream conditions have been plotted as a function of strength in figure 6. In this figure, it can be seen that the sonic condition is attained at $V_2 \approx 2.44V_c$. Beyond the sonic point, the discontinuities are

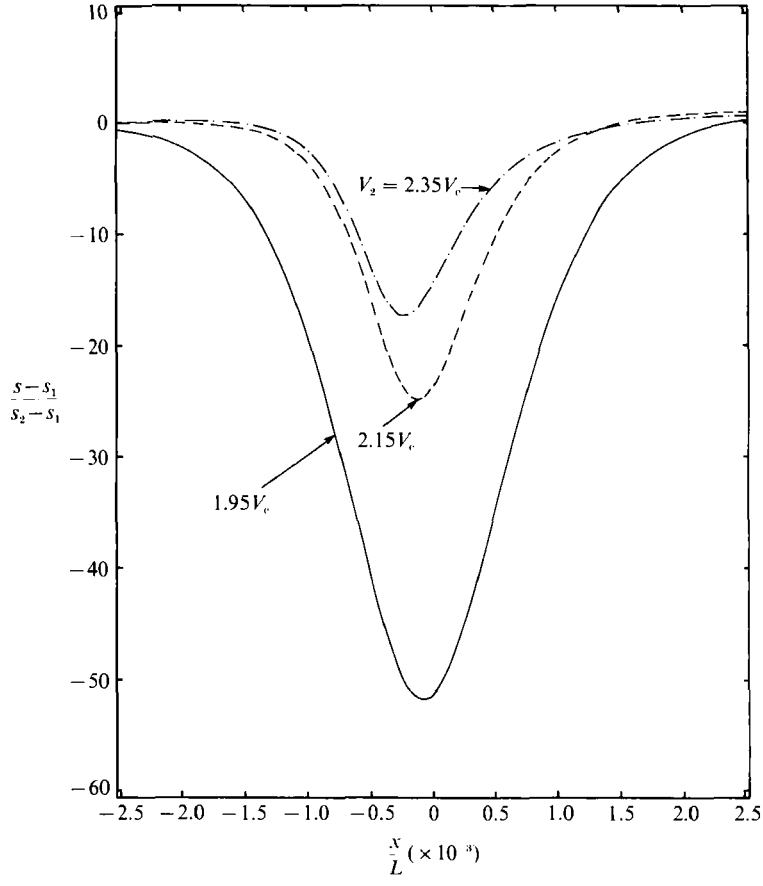

FIGURE 4. Variation of entropy *vs.* x for three expansion shocks in PP10. Numerical data are given in table 2.

inadmissible. These inadmissible conditions are indicated by dotted lines. This series of shocks has a local minimum in the thickness τ at about $V_2 = 2.2V_c$. The minimum is clearly evident in both figure 6 and table 2, thus providing some verification of results (ii) of the weak shock theory.

The physical mechanisms leading to this minimum shock thickness are fundamentally different than those leading to the well-known minimum found in the theory of perfect gases. The latter is due to the variation of the dissipation parameters through the shock layer and occurs at shock Mach numbers in neighbourhood of 3. In contrast, the local minimum reported here is due to the approach to sonic conditions. In fact, the minimum occurs even in numerical experiments that set the viscosity and thermal conductivity equal to constants. The local minimum was first discovered in the weak-shock theory that takes the dissipation parameters to be constant, at least to the lowest order in the perturbation scheme. Finally, it is of interest to note that the viscosities after the shock tend to decrease with shock strength $|(p_2-p_1)/p_1|$ if the shocks are of the expansion type. For example, the viscosities after the three shocks depicted in figures 3–5 are 3.0, 2.8, 2.6×10^{-5} kg/ms for the cases $V_2/V_c = 1.95$, 2.15, 2.35, respectively. The upstream

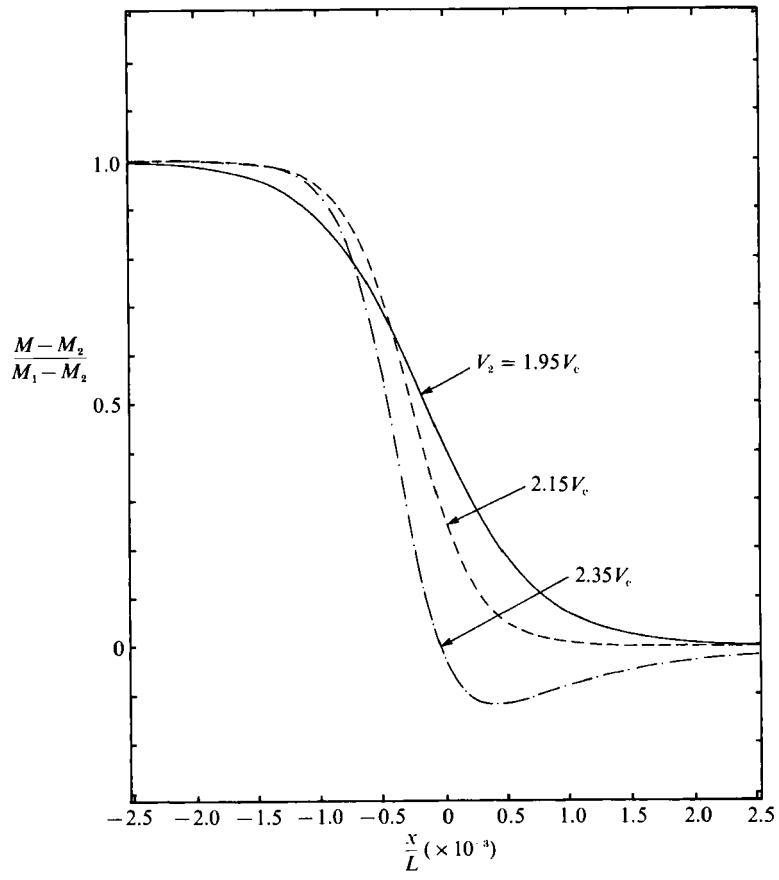

FIGURE 5. Variation of Mach number *vs.* x for three expansion shocks in PP10. Numerical data are given in table 2.

viscosity was 3.3×10^{-5} kg/ms. One would therefore expect the decreases in viscosity to combine with the increases in strength to prevent the occurrence of the local minimum which is actually observed.

The entropy variation also verifies the predictions of Cramer (1987*a*) as well as those given in §5 of the present article. Although $s < s_1$ over most of the shock layer, the non-dimensional entropy always becomes positive as the downstream conditions are approached. In table 2 it can be seen that the strongest shock crosses the $\Gamma = 0$ locus ($\Gamma_2 > 0$). As predicted by the weak-shock theory, the Mach-number variation for this shock has a local minimum there.

At this stage, it may be illuminating to give dimensional results for the thermodynamic variables. From tables 1 and 2 we find that the $V_2 = 2.35V_c$ shock results in dimensional pressure and temperature jumps of $p_2 - p_1 = -1.5$ atm. and $T_2 - T_1 = -4.0$ °C. The relatively small temperature drop is to be expected because of the large specific heats involved.

It was found that the reference viscosity μ_* was approximately 1.43×10^{-5} kg/ms. When this result is combined with the critical-point data recorded in table 1, we find that $L \approx 4.5 \times 10^{-10}$ m for PP10. The minimum thickness for this series of runs was

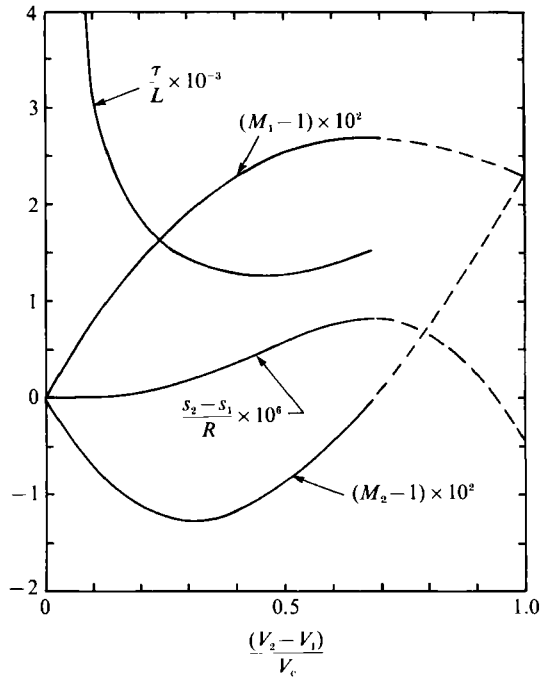

FIGURE 6. Variation of upstream and downstream Mach numbers, entropy jump and thickness with strength along a shock adiabat. Shocks are of the expansion type ($V_2 > V_1$) in PP10. The upstream state and value of μ_b are identical to those of figures 3–5.

approximately $1269L$ which occurred at $V_2 \approx 2.2V_c$. Thus, the minimum thickness for this upstream state and fluid is estimated to be 0.572 μm. If we estimate the mean free path at these temperatures using the standard hard-sphere, dilute-gas model, we find that this minimum shock thickness is about 33 times larger than the upstream mean free path. Furthermore, we expect the actual correlation lengths in the dense-gas regime to be considerably smaller than those based on the dilute-gas theory. Thus, we conclude that the results for this series of shocks are consistent with our continuum assumption.

The next series of shocks are relatively large-amplitude expansion shocks, the two strongest of which take the flow from one side of the negative-Γ region to the other. Thus, these are of the same general type as the double sonic shocks first described by Thompson & Lambrakis (1973). The pertinent numerical data are found in table 3 and the specific volume, entropy and Mach-number variations are depicted in figures 7–9. The shock adiabat is that marked $\hat{T} = 1.0$ in figure 2. Because Γ changes sign twice across the two strongest shocks, the weak-shock theory of Cramer & Kluwick (1984) and Cramer (1987*a*) is not expected to provide a qualitatively correct picture of the structure. Nevertheless, we again find a local minimum in the thickness and a negative entropy differential, i.e. $s < s_1$, over most of the shock layer. The main new feature is the local maximum and local minimum in the Mach number of the $V_2 = 2.4V_c$ and $V_2 = 2.6V_c$ shocks. A more detailed examination of the structure shows that these extrema occur near the $\Gamma = 0$ points. This appears to verify the general rule given in §5 of the present article, and that predicted earlier by Cramer (1987*a*) in the context of the Cramer–Kluwick approximation, which states that the Mach

$\frac{V_2}{V_c}$	$\frac{p_2}{p_c}$	$\frac{T_2}{T_c}$	$\frac{\Gamma_2\rho_2}{a_2}$	M_1	M_2	$\frac{s_2-s_1}{R}(\times 10^5)$	$\frac{\tau}{L}$
2.2	0.8745	0.9907	−0.010	1.040	0.965	45.17	476
2.4	0.8443	0.9892	0.101	1.047	0.975	68.20	459
2.6	0.8146	0.9878	0.196	1.050	0.990	84.09	490

TABLE 3. Numerical data for the expansion shocks of figures 6–8. Fluid is PP11 with $V_1 = 1.35V_c$, $T_1 = T_c$, $p_1 = 0.9944p_c$, $\rho_1\Gamma_1/a_1 = 0.242$ and $\mu_b/\mu = 0.5$.

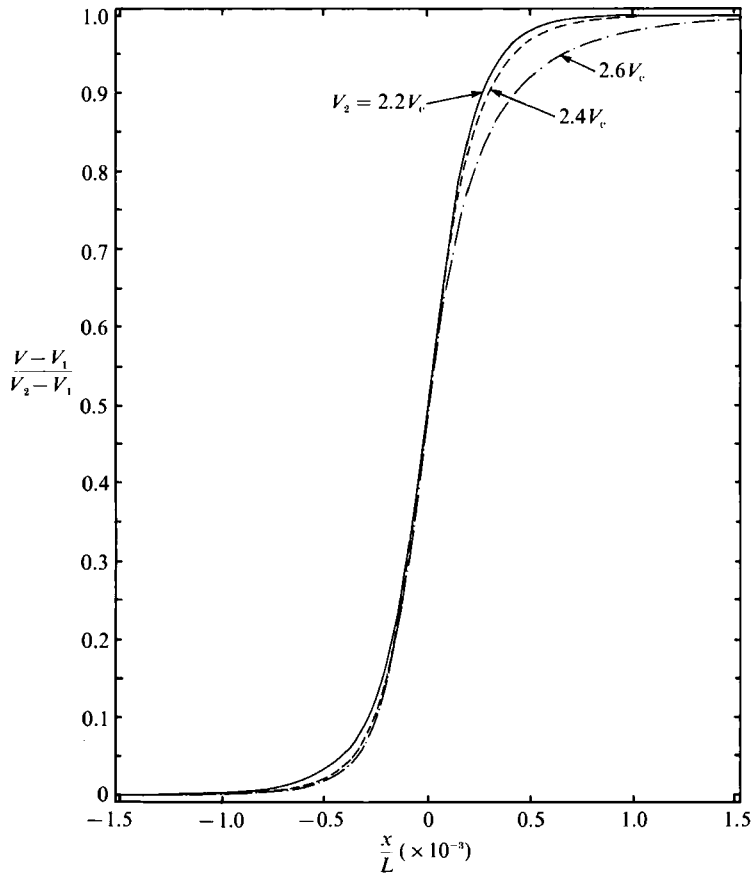

FIGURE 7. Variation of specific volume *vs.* x for three expansion shocks in PP11. Numerical data are given in table 3.

number always has an extremum near $\Gamma = 0$ points. Inspection of table 3 shows that the weakest shock involves only one sign change in Γ. As a result, the corresponding Mach number distribution in figure 9 has only the local maximum associated with the high-pressure $\Gamma = 0$ point.

Results which were completely unanticipated are represented in the next series of shocks. The fluid chosen was FC-71 and the upstream state was taken to be to the

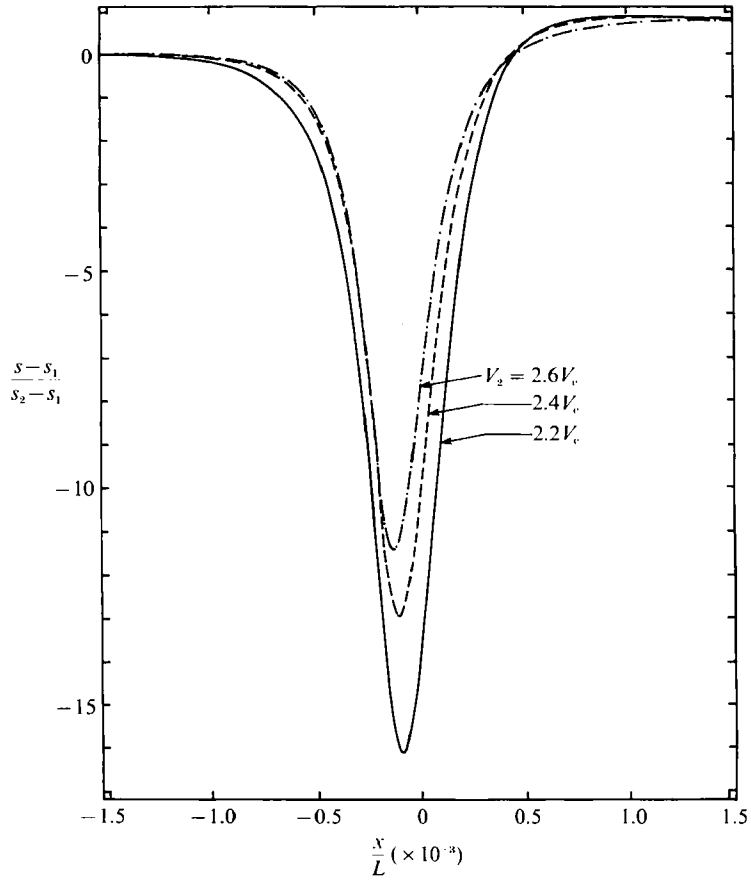

FIGURE 8. Variation of entropy *vs.* x for three expansion shocks in PP11. Numerical data are given in table 3.

right of the negative-Γ region in the (p, V)-diagram. The upstream state is given in the captions to figures 10–12 and to table 4. The shocks then take the flow all the way through the region of negative nonlinearity. The most dramatic new features are seen in figure 10. As the shocks become weaker (the weakest shock is that having $V_2 = 1.3V_c$) two additional inflexion points in the V *vs.* x curves become evident. Both the classical weak-shock theory and that of Cramer & Kluwick (1984) can only admit one inflexion point in the V *vs.* x curve. The entropy distribution plotted in figure 11 gives further clues to the process. The weakening of the shock leads to a splitting of the single hump ordinarily associated with the entropy variation. In fact, the weakest shocks appear to have undergone an internal splitting reminiscent of the shock splitting described by Cramer (1989*a*). We have, of course, checked the admissibility of this shock. The Rayleigh line was found to lie entirely above the adiabat. Thus, in terms of the inviscid theory, the shock appears as a single discontinuity. The explanation for this phenomenon is that we are approaching the shock-splitting condition (where the middle of the Rayleigh line first makes contact with the negative Γ-hump of the shock adiabat) as the shock is weakened. The internal structure is simply anticipating the inviscid splitting. For this reason, we refer to this phenomenon as impending shock splitting.

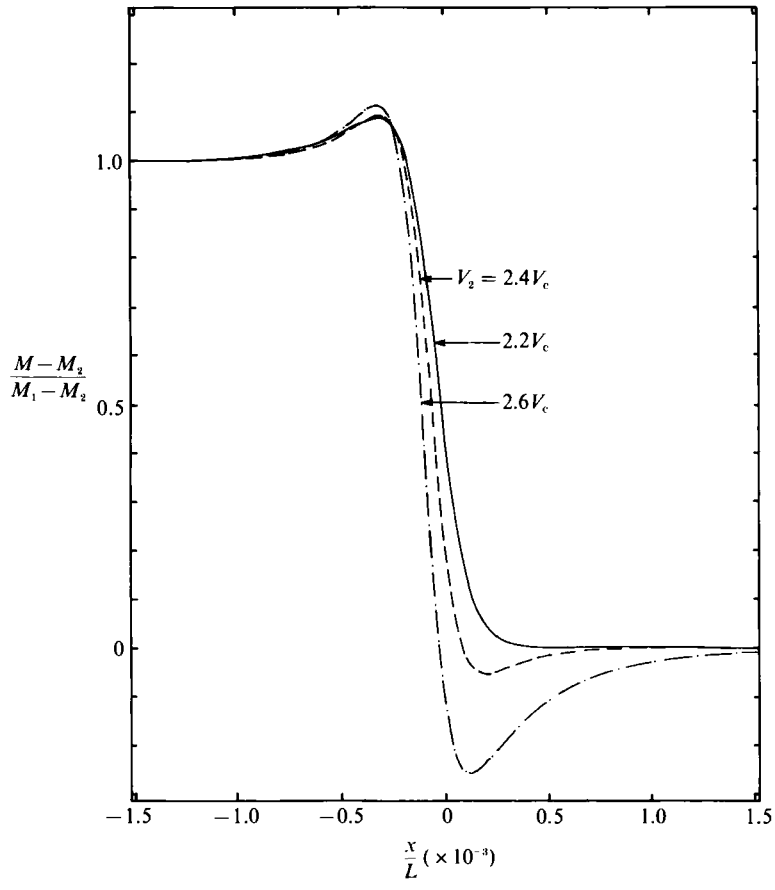

FIGURE 9. Variation of Mach number *vs.* x for three expansion shocks in PP11. Numerical data are given in table 3.

The phenomenon of impending shock splitting is similar to the thickening caused by the approach to sonic conditions in that it is primarily due to a change in nonlinear, rather than dissipative, effects as the admissibility limit is approached. We have verified that impending shock splitting also occurs even if the viscosities and thermal conductivity are taken to be constant. A further verification, which also illuminates the conditions under which impending shock splitting occurs, is described in the next section of the present paper.

A second new result is seen in the Mach-number distributions plotted in figure 12. In each case, the local maximum corresponds to a Mach number of 1.01 or larger. It appears that this class of shock can have an internal layer of supersonic flow, i.e. there will be three, instead of one, sonic points within the shock layer.

As the shock strength increases, the additional inflexion points in the V *vs.* x curves ultimately vanish and the entropy distribution returns to the classical single-hump configuration. The latter can already be seen in figure 11 although the extra inflexion points still appear in figure 10.

$\frac{V_2}{V_c}$	$\frac{p_2}{p_c}$	$\frac{T_2}{T_c}$	$\frac{\Gamma_2\rho_2}{a_2}$	M_1	M_2	$\frac{s_2-s_1}{R}\times 10^5$
1.3000	1.0528	1.0088	0.8330	1.017	0.949	13.94
1.2875	1.0551	1.0089	0.8979	1.017	0.942	18.04
1.2750	1.0575	1.0091	0.9644	1.018	0.934	22.82
1.2625	1.0599	1.0092	1.0322	1.019	0.926	28.36
1.2500	1.0624	1.0094	1.1011	1.020	0.917	34.76
1.2375	1.0649	1.0096	1.1707	1.021	0.907	42.10
1.2250	1.0675	1.0097	1.2408	1.022	0.897	50.50

TABLE 4. Numerical data for the compression shocks of figures 10–12. Fluid is FC-71 with $V_1 = 2.5V_c$, $T_1 = T_c$, $p_1 = 0.8523p_c$, $\rho_1\Gamma_1/a_1 = 0.2160$ and $\mu_b/\mu = 0$.

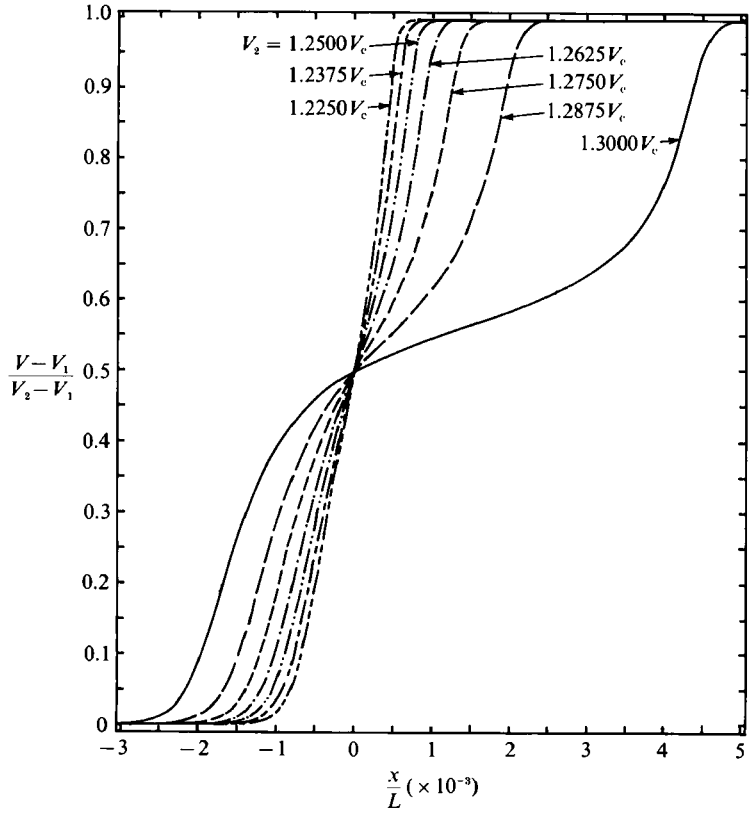

FIGURE 10. Variation of specific volume *vs.* x for seven compression shocks in FC-71. Numerical data are given in table 4.

5. A weak-shock approximation

We may gain further insight into the phenomenon of impending shock splitting by consideration of a weak-shock approximation. Both shock splitting and impending shock splitting occur only if Γ changes sign twice across the proposed discontinuity. In the following, we construct an extension of the weak-shock theory of Cramer &

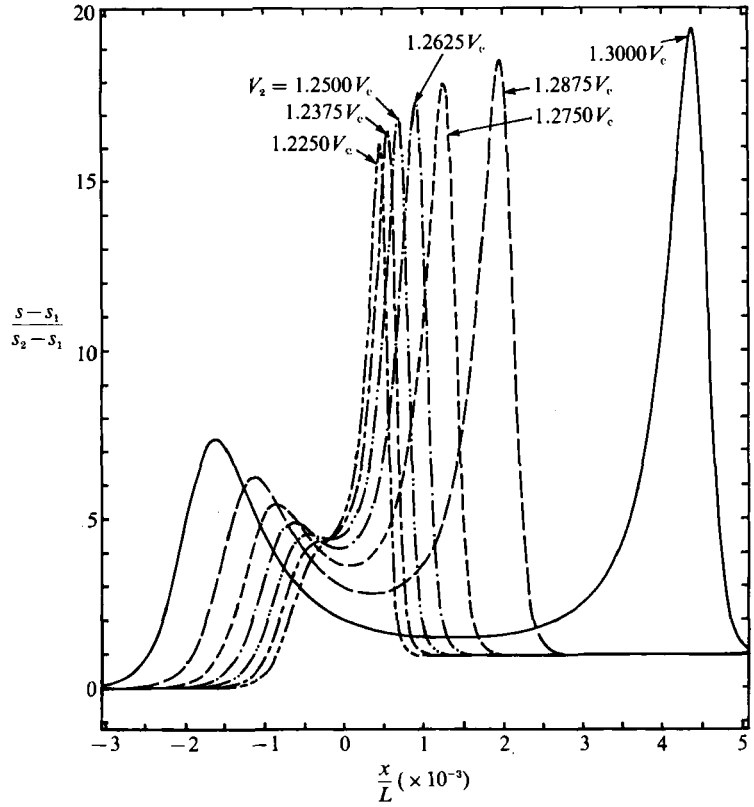

FIGURE 11. Variation of entropy *vs.* x for seven compression shocks in FC-71. Numerical data are given in table 4.

Kluwick (1984) which is capable of modelling such flows. As in the classical analysis of Lighthill (1956) and the work of Cramer & Kluwick (1984), Cramer (1987*a*) and Lee-Bapty & Crighton (1987), a Burgers equation is first derived. The dissipative structure is then obtained as an exact steady-state solution.

The model presented here takes the disturbances to be small, one-dimensional and unsteady, i.e.

$$\rho = \rho(x,t) \text{ only and } \frac{\rho-\rho_0}{\rho_0} = o(1). \tag{5.1}$$

The undisturbed state is taken to be at rest and uniform. If we further require that

$$\frac{\rho_0\Gamma_0}{a_0} = O\left(\frac{\rho-\rho_0}{\rho_0}\right)^2, \quad \frac{\rho_0^2}{a_0}\frac{\partial\Gamma}{\partial\rho}(\rho_0,s_0) = O\left(\frac{\rho-\rho_0}{\rho_0}\right), \quad \frac{\rho_0^3}{a_0}\frac{\partial^2\Gamma}{\partial\rho^2}(\rho_0,s_0) = O(1) \tag{5.2}$$

we find that the local value of Γ can have as many as two sign changes even though the disturbances are required to be small. We note that this is a natural extension of the classical theory

$$\frac{\rho_0\Gamma_0}{a_0} = O(1), \quad \frac{\rho-\rho_0}{\rho_0} = o(1)$$

and the theory of Cramer & Kluwick (1984)

$$\frac{\rho_0\Gamma_0}{a_0} = O\left(\frac{\rho-\rho_0}{\rho_0}\right) = o(1), \quad \frac{\rho_0^2}{a_0}\frac{\partial\Gamma}{\partial\rho}(\rho_0,s_0) = O(1).$$

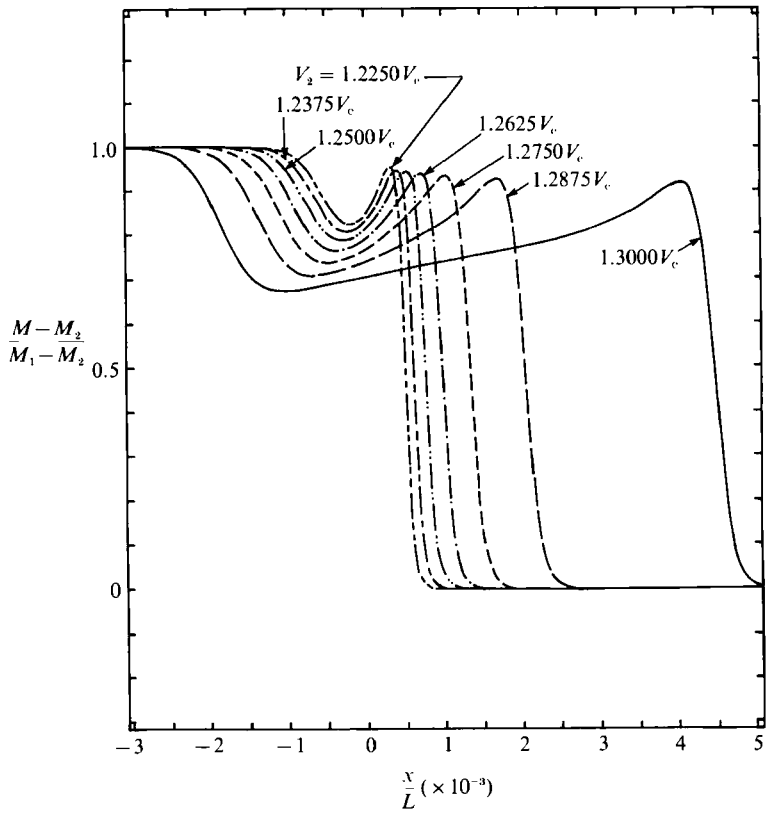

FIGURE 12. Variation of Mach number *vs.* x for seven compression shocks in FC-71. Numerical data are given in table 4.

It is easily verified that (5.2) is valid in the vicinity of the peak of the $\Gamma = 0$ locus where the isentropes are tangent to the $\Gamma = 0$ curve. Although the formal range of validity may appear to be rather narrow, the model presented here nevertheless gives a good qualitative picture of the general case while preserving the simplifications inherent in the small-disturbance approximation. One such simplification is that the entropy variations due to the shock waves may be neglected for the purposes of the calculation of most of the flow features. In fact, it is easily verified that the entropy rise is of the fifth order in the shock strength; this is found to be sufficiently small for the present purposes. This entropy rise is seen to be considerably smaller than either that found in the classical theory, where the entropy rise is of the third order, or that of the Cramer–Kluwick theory where the jump is of the fourth order. The assumption that the entropy rise is small is also borne out by the computational results. From table 4 it is seen that even the strongest shock corresponds to an entropy rise of only $5 \times 10^{-4}R$.

With such a small entropy rise, it is natural to expect that reflected waves caused by variations in the shock strength are also negligible. For the purposes of constructing the Burgers equation we will assume that this is the case. However, this is not formally necessary for the analysis of the dissipative structure which can be carried out in the context of shocks of constant strength. With the neglect of reflected

waves we may take the disturbances to be right-moving simple waves having a local convected sound speed given by

$$\sigma(\rho) = w + a = w' + a' + \int_{\rho'}^{\rho} \Gamma(r, s')\,\mathrm{d}r, \tag{5.3}$$

where w is the particle velocity and primes denote an arbitrary reference state. Result (5.3) was given by Cramer & Sen (1986) although an equivalent form is found in the earlier work of Thompson & Lambrakis (1973). We note that (5.3) is strictly valid only if the flow is inviscid. Dissipative effects will be considered once the nonlinearity is properly taken into account. If the assumptions (5.1) and (5.2) are applied to (5.3), we find that the local convected sound speed may be approximated by

$$\frac{\sigma}{a_0} = 1 + \frac{\rho_0 \Gamma_0}{a_0}\frac{\rho-\rho_0}{\rho_0} + \tfrac{1}{2}A\left(\frac{\rho-\rho_0}{\rho_0}\right)^2 + \tfrac{1}{6}\Xi\left(\frac{\rho-\rho_0}{\rho_0}\right)^3 + O\left(\frac{\rho-\rho_0}{\rho_0}\right)^4, \tag{5.4}$$

where the reference state was taken to be the stationary and uniform undisturbed state, i.e. $w' = 0$, $\rho' = \rho_0$, $s' = s_0$, and

$$A \equiv \frac{\rho_0^2}{a_0}\frac{\partial \Gamma}{\partial \rho}(\rho_0, s_0), \Xi \equiv \frac{\rho_0^3}{a_0}\frac{\partial^2 \Gamma}{\partial \rho^2}(\rho_0, s_0). \tag{5.5}$$

We note that A is just the second nonlinearity coefficient introduced by Cramer & Kluwick (1984). In deriving (5.4) from (5.3) a Taylor series for $\Gamma(\rho, s)$ was employed. The fact that the entropy rise is of the fifth order in $(\rho-\rho_0)$ was also used. Because of (5.2) the terms proportional to $\rho_0\Gamma_0/a_0$, A, and Ξ in (5.4) are all of order $((\rho-\rho_0)/\rho_0)^3$; thus, each must be included in the lowest-order nonlinear theory. An inviscid Burgers equation corresponding to (5.4) is

$$\frac{\partial}{\partial t}\left(\frac{\rho-\rho_0}{\rho_0}\right) + \sigma(\rho)\frac{\partial}{\partial x}\left(\frac{\rho-\rho_0}{\rho_0}\right) = 0, \tag{5.6}$$

where $\sigma(\rho)$ is given by (5.4). Application of the method of characteristics to (5.6) verifies that

$$\rho = \text{constant on lines } \frac{\mathrm{d}x}{\mathrm{d}t} = \sigma(\rho). \tag{5.7}$$

Dissipative effects may be taken into account in the same manner as in the classical theory and the Cramer–Kluwick theory. Here we assume that the spatial lengthscales are such that the dissipative terms are in a rough balance with the nonlinear terms. More precisely we take

$$l = O\left\{\frac{\mu_0}{\rho_0 a_0}\left(\frac{\rho_0}{\rho-\rho_0}\right)^3\right\}, \tag{5.8}$$

where l is some measure of the lengthscale of the disturbance. In effect, (5.8) requires that the wave Reynolds number $l\rho_0 a_0/\mu_0$ is of the order of the inverse third power of the non-dimensional disturbance amplitude. The dissipative form of (5.6) may then be written

$$\frac{\partial}{\partial t}\left(\frac{\rho-\rho_0}{\rho_0}\right) + \sigma(\rho)\frac{\partial}{\partial x}\left(\frac{\rho-\rho_0}{\rho_0}\right) = \tfrac{1}{2}\delta\frac{\partial^2}{\partial x^2}\left(\frac{\rho-\rho_0}{\rho_0}\right), \tag{5.9}$$

where

$$\delta \equiv \frac{\mu_0}{\rho_0}\left\{\frac{\mu_{b0}}{\mu_0} + \frac{4}{3} + \frac{\gamma_0 - 1}{Pr_0}\right\} \tag{5.10}$$

is a form of the acoustic diffusivity, Pr is the Prandtl number and γ is the ratio of specific heats. Because k, μ, μ_b, c_p, $\gamma-1>0$, it may be shown that $\delta>0$.

Equation (5.9) may be used to examine the evolution of arbitrary disturbances in a manner similar to the classical theory or the theory of Cramer & Kluwick (1984). As indicated earlier in this section, we shall focus our attention on shock-like solutions. We first transform to a coordinate system moving with a constant shock speed $\mathscr{S}$. In such a system, (5.9) may be rewritten as

$$\frac{\partial u}{\partial t}+(\sigma-\mathscr{S})\frac{\partial u}{\partial \xi}=\tfrac{1}{2}\delta\frac{\partial^2 u}{\partial \xi^2}, \tag{5.11}$$

where

$$u\equiv\frac{\rho-\rho_0}{\rho_0\epsilon}, \quad \xi=x-\mathscr{S}t, \tag{5.12}$$

and ϵ is a small parameter measuring the maximum amplitude of the density perturbation. The structure is obtained by taking the flow to be steady, i.e. $\partial u/\partial t=0$, in (5.11) and by requiring that u satisfies

$$\begin{aligned} u&\to u_1 \quad \text{as} \quad \xi\to\infty,\\ u&\to u_2 \quad \text{as} \quad \xi\to-\infty, \end{aligned} \tag{5.13}$$

which are seen to be the analogues of (2.3). The equation governing the shock structure therefore reads

$$\tfrac{1}{2}\Lambda\ddot{u}=(Q'-\sigma)\dot{u}, \tag{5.14}$$

where dots denote differentiation with respect to a scaled ξ defined by

$$\hat{\xi}\equiv\frac{\xi}{l}. \tag{5.15}$$

The quantity σ is a non-dimensional measure of the shock speed defined by

$$\sigma\equiv\frac{\mathscr{S}-a_0}{\epsilon^3 a_0}=O(1). \tag{5.16}$$

The quantity $Q=Q(u)$ is defined

$$Q\equiv\tfrac{1}{2}\hat{\Gamma}u^2+\tfrac{1}{6}\hat{\Lambda}u^3+\tfrac{1}{24}\Xi u^4 \tag{5.17}$$

so that

$$\frac{\sigma-a_0}{\epsilon^3 a_0}=Q'(u)\equiv\frac{\mathrm{d}Q}{\mathrm{d}u}=\hat{\Gamma}u+\tfrac{1}{2}\hat{\Lambda}u^2+\tfrac{1}{6}\Xi u^3, \tag{5.18}$$

where

$$\hat{\Gamma}\equiv\frac{\rho_0\Gamma_0}{a_0}\frac{1}{\epsilon^2}=O(1), \quad \hat{\Lambda}\equiv\frac{\Lambda}{\epsilon}=O(1). \tag{5.19}$$

Throughout we have noted that (5.13) introduces no natural geometric lengthscale and have therefore set

$$l\equiv\frac{\mu_0}{a_0\epsilon^3\rho_0},$$

so that

$$\Lambda\equiv\frac{\delta}{l\epsilon^3 a_0}=\frac{\mu_{b0}}{\mu_0}+\frac{4}{3}+\frac{\gamma_0-1}{Pr_0}=O(1). \tag{5.20}$$

The function $Q(u)$ is closely related to the shock adiabat or, because the entropy variations are so small, the isentropes. A typical Q-curve is sketched in figure 13 for

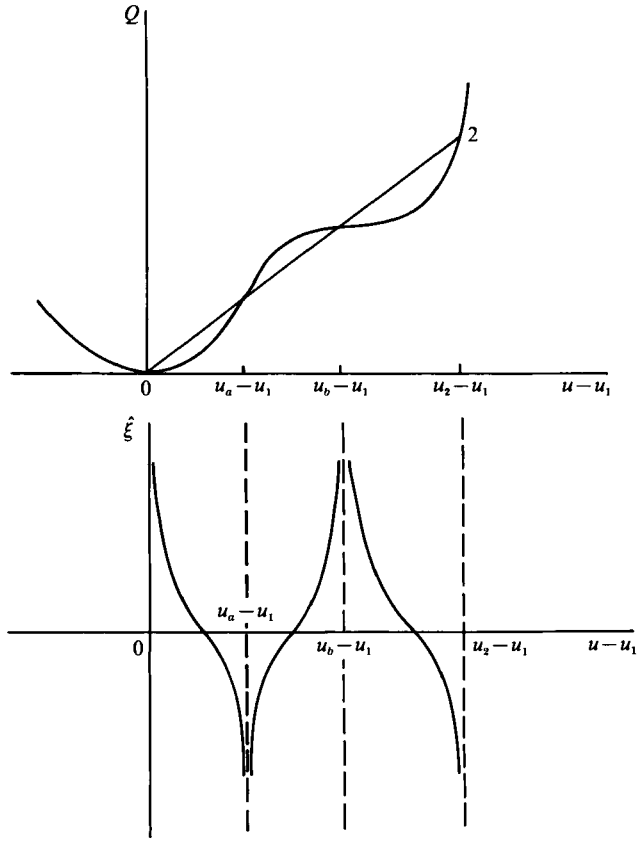

FIGURE 13. Sketch of a typical Q-curve and solutions to (5.25) or (5.26) for upstream and downstream states given by u_1 and u_2, respectively. At $u = u_1$, u_a, u_b, and u_2, the right-hand side of (5.26) vanishes.

an undisturbed state which is somewhat to the right of the $\Gamma = 0$ locus in the (p, V)-diagram. As indicated by (5.18), the slope of this curve, i.e. Q', is simply a scaled version of the convected sound speed. If we differentiate (5.18), we find that the second derivative is just

$$Q'' = \hat{\Gamma} + \hat{A}u + \tfrac{1}{3}\Xi u^2 \tag{5.21}$$

which can be shown to be a scaled version of the local value of the fundamental derivative. This could have been anticipated from (5.3). Thus, $\Gamma < 0$ where the curvature of the Q-curve is downward ($Q'' < 0$) and $\Gamma > 0$ where $Q'' > 0$.

The shock speed σ is determined by consideration of the first integral of (5.14). Integration with respect to $\hat{\xi}$ and application of (5.13) yields

$$\sigma = \frac{[Q]}{[u]} \tag{5.22}$$

as the expression for the shock speed. The original structure equation (5.14) and its first integral therefore reads

$$\tfrac{1}{2}\Delta\ddot{u} = \left(Q' - \frac{[Q]}{[u]}\right)\dot{u}, \tag{5.23}$$

$$\tfrac{1}{2}\Delta\dot{u} = \left(\frac{Q-Q_1}{u-u_1} - \frac{[Q]}{[u]}\right)(u-u_1). \tag{5.24}$$

In the exact theory of shock waves, the analogue of (5.22) is just (2.6). That is, the shock speed is proportional to (in the weak-shock theory it is equal to) the slope of the Rayleigh line connecting the upstream and downstream states. (Here we shall refer to straight lines in the (Q, u)-plane as Rayleigh lines owing their close relationship to those introduced previously.) Furthermore, (5.24) is recognized as the weak-shock analogue of the original system (2.1).

The general features of the dissipative structure are easily deduced by inspection of (5.13), (5.22)–(5.24). From (5.24) it is clear that $\dot{u} \to 0$ whenever

$$\frac{\hat{Q}-Q_1}{\hat{u}-u_1} = \frac{[Q]}{[u]}, \tag{5.25}$$

where $\hat{Q} \equiv Q(\hat{u})$. The solutions $\hat{u}$ to (5.25) can be shown to be the values of u at which the Rayleigh line connecting (u_1, Q_1) to (u_2, Q_2) intersects the Q *vs.* u curve. We therefore obtain the analogue of the general existence condition stated in §2. This may be stated as follows: smooth solutions to (5.23) or (5.24) exist if and only if the straight line connecting u_1 to u_2 lies entirely above or below the Q *vs.* u curve between u_1 and u_2. Typical inadmissible discontinuities are represented by figure 13 where the resultant singular solutions are also sketched. The intermediate intersections are at u_a and u_b in this figure. If no intermediate intersections occur, the proposed transition is smooth, i.e. acceptable, and the direction of the jump is determined by requiring the satisfaction of (5.13).

The distinguishing feature of impending shock splitting will be the occurrence of multiple inflexion points in the u *vs.* $\hat{\xi}$ curve. Inspection of (5.23) shows that an inflexion point will occur at values of u where the slope of the straight line connecting the upstream and downstream states is parallel to the Q *vs.* u curve. It is easily verified that most admissible shocks therefore have only one inflexion point in the u *vs.* $\hat{\xi}$ distribution. However, multiple solutions to

$$\frac{[Q]}{[u]} = Q'(u) \tag{5.26}$$

are possible for a range of admissible compression shocks which take the flow from one side of the $\Gamma < 0$ region to the other. In figure 14 the downstream state of these shocks is between u_a and u_b. For this range of shock strengths, there will be three points at which (5.26) is satisfied and therefore three inflexion points in the u *vs.* $\hat{\xi}$ curve even though the shock appears as a single discontinuity from the point of view of the inviscid theory. The state denoted by b is such that the slope of the Rayleigh line from state 1 to b is parallel to the slope of the Q-curve at the left-most inflexion point i', i.e.

$$\left.\frac{[Q]}{[u]}\right|_{u_1 \to u_b} = Q'(u_{i'}).$$

Note that $Q'(u_{i'}) > Q'(u_{i''})$ for all values of $\hat{\Gamma}, \Lambda, \Xi$ leading to shock splitting. Stronger shocks having $u_2 > u_b$ have only one solution to (5.26) and therefore only one inflexion point. Thus, away from the neighbourhood of the shock-splitting condition, the structure appears similar to the classical case. The state denoted by a is the weakest admissible shock that can take the flow from one side of the $\Gamma < 0$ region to the other. Downstream conditions below the lower limit (u_a) will result in an intermediate intersection and therefore will be inadmissible. Inadmissible discontinuities having $u_{i''} < u_2 < u_a$ will result in shock splitting. These observations are

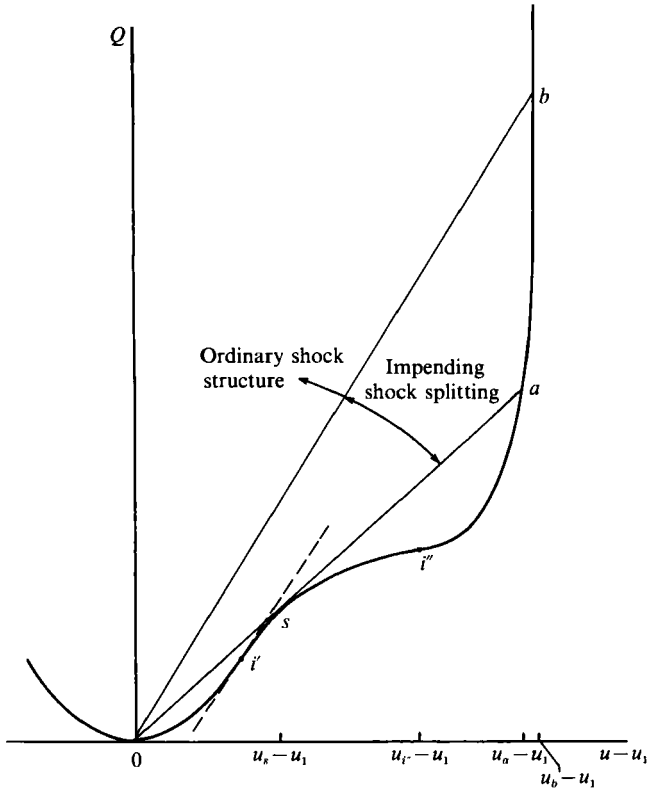

FIGURE 14. Sketch to illustrate conditions for impending shock splitting. The u *vs.* $\hat{\xi}$ curve has inflexion points at values of $u_1 < u < u_2$ whenever the tangent to the Q *vs.* u curve is parallel to the Rayleigh line between (u_1, Q_1) and (u_2, Q_2).

in complete accord with the numerical calculations and we therefore conclude that the density distributions illustrated in figure 10 can be anticipated through use of the present weak-shock model.

The entropy distribution can also be shown to be in agreement with the computations presented in §4. If the energy equation is cast in terms of the entropy, s, we find that

$$\rho T\left(\frac{\partial s}{\partial t}+w\frac{\partial s}{\partial x}\right) = (\mu_b+\tfrac{4}{3}\mu)\left(\frac{\partial w}{\partial x}\right)^2+\frac{\partial}{\partial x}\left(k\frac{\partial T}{\partial x}\right) \tag{5.27}$$

is the exact equation for the entropy distribution in the shock. If we make the assumption that the flow is steady in the reference frame moving with the shock and make the weak-shock approximation we find that (5.27) can be approximated by

$$\dot{s} = -\beta_0 a_0^2 \frac{\epsilon^4}{Pr_0}\ddot{u}, \tag{5.28}$$

where dots again denote differentiation with respect to $\hat{\xi}$ and β is the coefficient of thermal expansivity defined by

$$\beta \equiv -\frac{1}{\rho}\frac{\partial \rho}{\partial T}\bigg|_p.$$

Throughout we shall take $\beta > 0$. Integration and use of (5.13) yields

$$\frac{s-s_1}{\beta_0 a_0^2} = -\frac{\epsilon^4}{Pr_0}\dot{u}. \tag{5.29}$$

Thus, the entropy has a local maximum or minimum at each inflexion point of the u *vs.* $\hat{\xi}$ curve. The entropy distribution will have two maxima and one local minimum when impending shock splitting occurs; this is in qualitative agreement with the results presented in §4. The result (5.29) is essentially the same as that employed by Cramer (1987*a*). We may also conclude that all admissible expansion shocks have a local minimum, rather than maximum, in the entropy distribution, at least in the context of this weak-shock theory.

In the frame moving with the shock, the exact expression for the Mach number M is

$$M-1 = \frac{\mathscr{S}-\sigma}{a}, \tag{5.30}$$

where $\sigma = \sigma(\rho)$ is given by (5.3). If we approximate σ and $\mathscr{S}$ using (5.16), (5.18) and (5.22) and note that a may be approximated as a_0, we find that (5.30) can be written

$$M-1 \approx \epsilon^3(\mathscr{I}-Q'(u)) = \epsilon^3\left(\frac{[Q]}{[u]}-Q'(u)\right). \tag{5.31}$$

If we differentiate (5.31) with respect to u we find that

$$\frac{\mathrm{d}M}{\mathrm{d}u} = -\epsilon^3 Q''. \tag{5.32}$$

By combining (5.32) with (5.21) it can be shown that M has a local maximum or minimum whenever the local value of Γ changes sign. This agrees with result (ii) from the Cramer–Kluwick theory and is in qualitative agreement with the finite-amplitude results reported in §4 of the present article.

Equation (5.31) may also be employed to show that any acceptable shock, i.e. any discontinuity having a smooth structure satisfying (5.23) and (5.13), takes the flow from supersonic to subsonic conditions as measured in a frame where the shock appears stationary.

Finally, we note that (5.31) may be combined with (5.23) to show that

$$M-1 = -\tfrac{1}{2}\Delta\epsilon^3\frac{\ddot{u}}{\dot{u}}.$$

Thus, the flow is sonic at each inflexion point in the u *vs.* $\hat{\xi}$ curve. In the case of impending shock splitting there will be three sonic points. Because the flow is necessarily supersonic upstream of the shock and subsonic downstream, we conclude that there will always be an embedded region of supersonic flow in any shock layer corresponding to impending shock splitting. Just such an embedded region was found in the numerical computations described in §4.

To conclude this section, we note that (5.24) can be integrated to obtain explicit solutions for $\hat{\xi} = \hat{\xi}(u; u_1, u_2, \hat{\Gamma}, \hat{\Lambda}, \Xi)$. If we factor (5.24) and take $\hat{\xi} = 0$ at $u = \frac{1}{2}(u_1+u_2)$, we find that

$$\frac{\Xi}{12\Delta}\hat{\xi} = \int_{\frac{1}{2}(u_1+u_2)}^{u} \frac{\mathrm{d}u}{(u-u_1)(u-u_2)(u^2+\alpha_1 u+\alpha_2)}, \tag{5.33}$$

where

$$\left.\begin{aligned}\alpha_1 &\equiv u_1+u_2+4\frac{\hat{\Lambda}}{\Xi},\\ \alpha_2 &\equiv u_2^2+u_2\left(u_1+4\frac{\hat{\Lambda}}{\Xi}\right)+u_1^2+4u_1\frac{\hat{\Lambda}}{\Xi}+12\frac{\hat{\Gamma}}{\Xi}.\end{aligned}\right\} \tag{5.34}$$

The significance of the quadratic $u^2+\alpha_1 u+\alpha_2$ is that its zero yields the other two roots of (5.25); these read

$$u^{\pm} = -\tfrac{1}{2}\alpha_1 \pm (\tfrac{1}{4}\alpha_1^2-\alpha_2)^{\frac{1}{2}}, \tag{5.35}$$

provided $\alpha_1^2 > 4\alpha_2$. Examples of such additional roots are points (u_a, Q_a) and (u_b, Q_b) in figure 13. Note that there are only two intersections of the Rayleigh line and the Q-curve in figure 14. Thus, $\alpha_1^2 < 4\alpha_2$ for this (u_1, u_2) pair. Upon integration of (5.33) we find

$$\begin{aligned}\frac{\Xi\hat{\xi}}{12\Lambda} &= B_1\ln\left(\frac{u_2-u}{u-u_1}\right)-B_2\ln\left(2\frac{u-u_1}{u_2-u_1}\right)+B_2\ln\left\{\frac{(u+\frac{1}{2}\alpha_1)^2+B_4^2}{[\frac{1}{2}(u_1+u_2+\alpha_1)]^2+B_4^2}\right\}^{\frac{1}{2}}\\ &\quad+\frac{1}{B_4}(B_3-B_2\tfrac{1}{2}\alpha_1)\left\{\tan^{-1}\left(\frac{2u+\alpha_1}{2B_4}\right)-\tan^{-1}\left(\frac{u_1+u_2+\alpha_1}{2B_4}\right)\right\}\end{aligned} \tag{5.36}$$

provided that $4\alpha_2 > \alpha_1^2$ and

$$\begin{aligned}\frac{\Xi\hat{\xi}}{12\Lambda} &= B_1\ln\left(\frac{u_2-u}{u-u_1}\right)-B_2\ln\left(2\frac{u-u_1}{u_2-u_1}\right)+B_2\ln\left\{\frac{(u-u^+)(u-u^-)}{(\frac{1}{2}(u_1+u_2)-u^+)[\frac{1}{2}(u_1+u_2)-u^-]}\right\}^{\frac{1}{2}}\\ &\quad+\frac{1}{B_5}(B_3-B_2\tfrac{1}{2}\alpha_1)\ln\left\{\frac{u-u^+}{u-u^-}\frac{\frac{1}{2}(u_1+u_2)-u^-}{\frac{1}{2}(u_1+u_2)-u^+}\right\}^{\frac{1}{2}},\end{aligned} \tag{5.37}$$

if $\alpha_1^2 > 4\alpha_2$, where $u^{\pm}$ are given by (5.35) and

$$B_1 = \frac{u_1^2+\alpha_1 u_1+\alpha_2}{B_6}, \tag{5.38}$$

$$B_2 = (u_2-u_1)\frac{\alpha_1+u_1+u_2}{B_6}, \tag{5.39}$$

$$B_3 = (u_2-u_1)\frac{\alpha_1 u_2+u_1 u_2-\alpha_2+\alpha_1^2+u_1\alpha_1}{B_6}, \tag{5.40}$$

$$B_4 = (\alpha_2-\tfrac{1}{4}\alpha_1^2)^{\frac{1}{2}}, \tag{5.41}$$

$$B_5 = (\tfrac{1}{4}\alpha_1^2-\alpha_2)^{\frac{1}{2}}, \tag{5.42}$$

$$B_6 = (u_2-u_1)(u_1^2+\alpha_1 u_1+\alpha_2)(u_2^2+\alpha_1 u_2+\alpha_2). \tag{5.43}$$

In the first case, i.e. $4\alpha_2 > \alpha_1^2$, the only singularities in $\hat{\xi}$ are at $u = u_1$ or u_2. In the second case, the intermediate singularities depicted in figure 13 occur if either u^+ or u^- fall between u_1 and u_2.

The two solutions (5.36) and (5.37) are rendered invalid if any one of the following conditions holds:

$$B_6 = 0, \tag{5.44}$$

$$B_4 \quad \text{or} \quad B_5 = 0, \tag{5.45}$$

$$u^{\pm} = \tfrac{1}{2}(u_1+u_2). \tag{5.46}$$

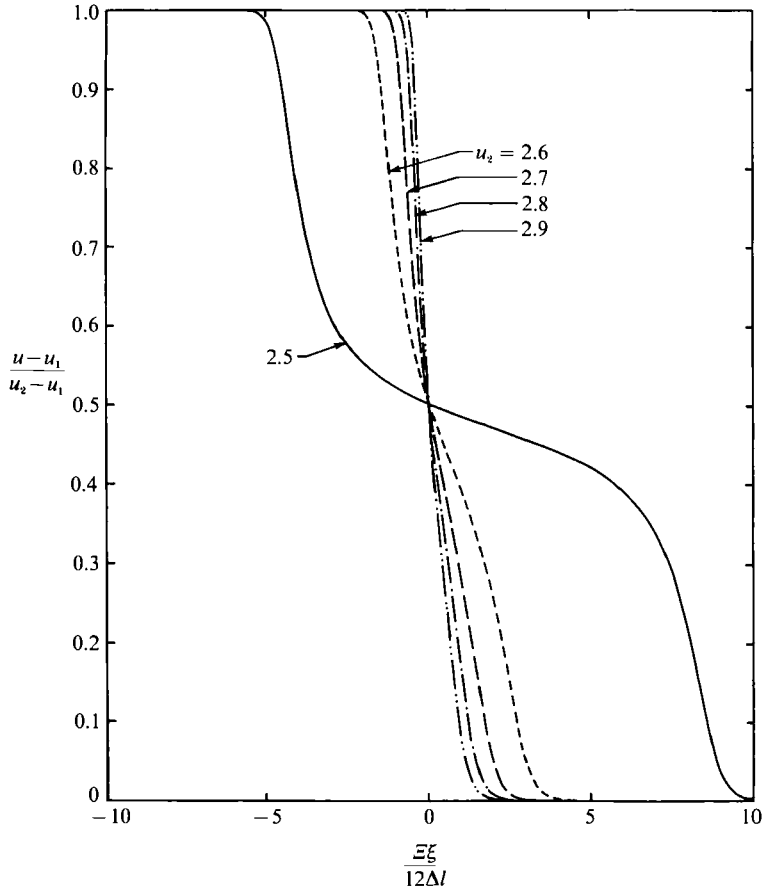

FIGURE 15. Variation of u *vs.* ξ according to the weak-shock approximation. The upstream conditions are on the right. The nonlinearity parameters and upstream value of u_1 were taken as $\hat{\Gamma} = 1$, $\hat{A} = -2$, $\Xi = 1.65$, $u_1 = 0$.

The last condition holds only if u^+ or u^- lies between u_1 and u_2; this, of course, does not occur in admissible shocks. The significance of condition (5.44) is seen by noting that B_6 may be rewritten as

$$B_6 = (u_2-u_1)(u_1-u^+)(u_1-u^-)(u_2-u^+)(u_2-u^-)$$

if $\alpha_1^2 > 4\alpha_2$. Thus, for $u_1 \neq u_2$, condition (5.44) holds only if one or the other intersection point $u^\pm$ merges with either the upstream or downstream conditions. It is easily verified that this is a tangency, i.e. sonic, point. It may also be shown that the approach to the sonic asymptote is algebraic rather than exponential; this, of course, is completely consistent with the more limited theory of Cramer & Kluwick (1984), Cramer (1987*a*) and Lee-Bapty & Crighton (1987). Substitution of condition (5.45) in (5.35) shows that

$$u^+ = u^- = -\tfrac{1}{2}\alpha_1$$

when either of (5.45) are satisfied. In this case the shock between u_1 and u_2 is non-sonic but the Rayleigh line turns out to be tangent to the Q-curve at $u = -\frac{1}{2}\alpha_1$. If $-\frac{1}{2}\alpha_1$ lies between u_1 and u_2, this is the condition for shock splitting; an example of

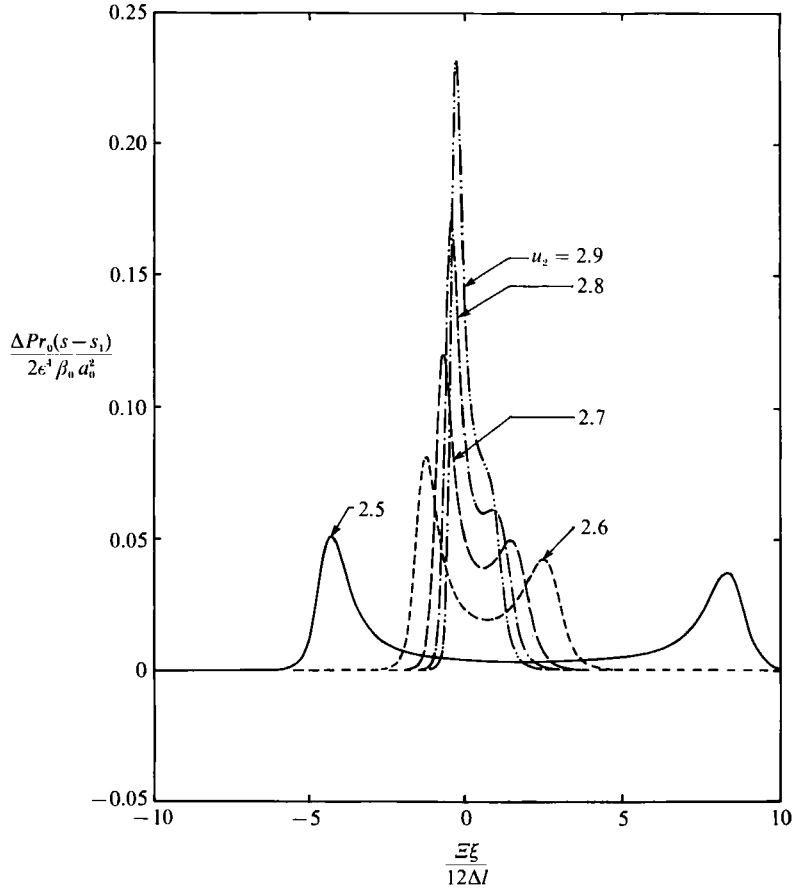

FIGURE 16. Variation of entropy *vs.* ξ according to the weak shock approximation. The upstream conditions are on the right. The nonlinearity parameters and upstream value of u_1 were taken as $\hat{\Gamma} = 1$, $\hat{A} = -2$, $\Xi = 1.65$, $u_1 = 0$.

this case is point s in figure 14. The solution to (5.45) is equivalent to the equation $\alpha_1^2 = 4\alpha_2$ which yields a quadratic for the shock strength $u_2 - u_1$ in terms of u_1 (or u_2), $\hat{\Gamma}$, $\hat{A}$, Ξ. There are two real solutions to the quadratic provided that

$$16\frac{\hat{A}^2}{\Xi^2} - 4\frac{\hat{A}}{\Xi}u_1 - 2u_1^2 > 36\frac{\hat{\Gamma}}{\Xi}.$$

It is a straightforward exercise to derive the limiting form of (5.36)–(5.42) when (5.45) holds. The main modification is to the last term in (5.36) and (5.37). The limiting form of this term is found to be

$$(B_3 - \tfrac{1}{2}\alpha_1 B_2)\left\{\frac{1}{\frac{1}{2}(u_1+u_2)+\frac{1}{2}\alpha_1} - \frac{1}{u+\frac{1}{2}\alpha_1}\right\}, \tag{5.47}$$

where B_2, B_3, and α_1 are all evaluated at the appropriate value of u_2. If $u^+ = u^- = -\frac{1}{2}\alpha_1$ are not between u_1 and u_2, the above term is bounded for all u between u_1 and u_2 and the solution is smooth. However, it is clear from (5.47) that $|\hat{\xi}| \to \infty$ as

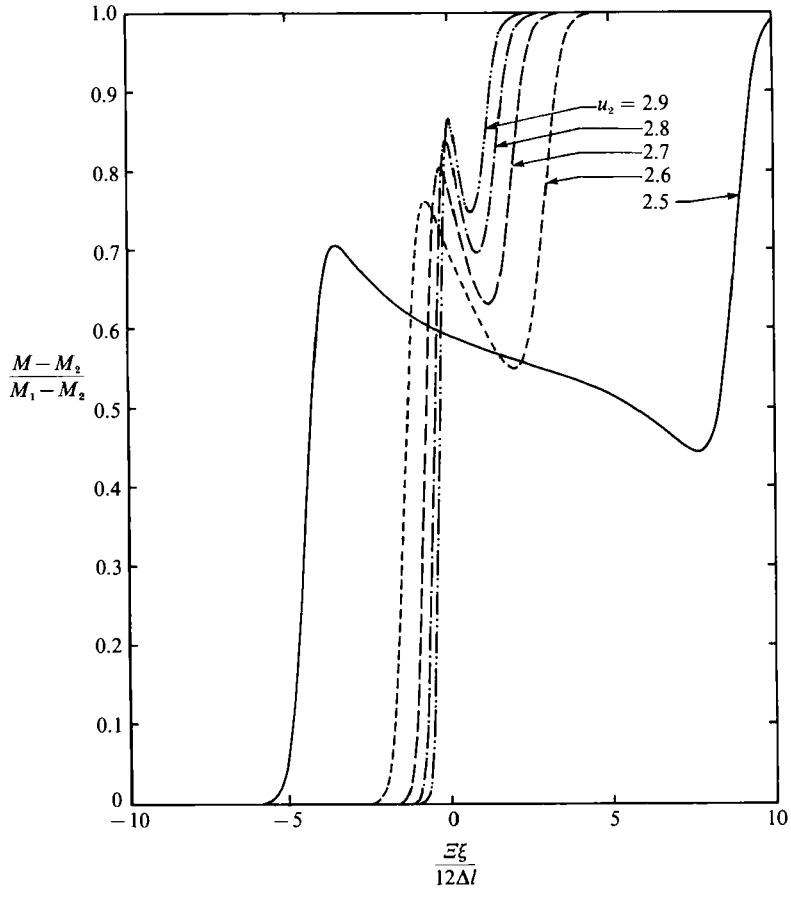

FIGURE 17. Variation of Mach number *vs.* ξ according to the weak shock approximation. The upstream conditions are on the right. The nonlinearity parameters and upstream value of u_1 were taken as $\hat{\Gamma} = 1$, $\hat{A} = -2$, $\Xi = 1.65$, $u_1 = 0$.

$u \to -\frac{1}{2}\alpha_1$ when $u^+ = u^- = -\frac{1}{2}\alpha_1$ is between u_1 and u_2. In terms of figure 14, this internal singularity occurs as $u \to u_s$. This, of course, is just the shock-splitting condition and could have been anticipated directly from our analysis of (5.24). Thus, as shock splitting is approached, the slope of the u *vs.* ξ curve at the middle inflexion point becomes horizontal and the shock thickness becomes infinite.

The density, entropy and Mach-number distributions for conditions corresponding to impending shock splitting are plotted in figures 15–17. The undisturbed state was chosen to be on the low-density side of the $\Gamma < 0$ region; this, of course, is similar to the upstream state of figures 10–12. For these values of u_1, Γ, $\hat{A}$, Ξ, impending shock splitting corresponds to values of u_2 between 2.48 and 2.83, approximately. Thus, the four weakest shocks give rise to impending shock splitting whereas the strongest shock is similar to that of the classical theory. These results are seen to be in complete agreement with the more general deductions of this section and are also in excellent qualitative agreement with the numerical results for finite-strength waves presented in §4.

6. Conclusions

The main objective of this study was to provide detailed descriptions of the dissipative structure of finite-amplitude shocks in single-phase fluids which have large specific heats. Particular attention is paid to the dense-gas regime. The standard continuum model is employed with state-of-the-art models for the equation of state and density dependencies of the shear viscosity and thermal conductivity.

Our computations confirm the existence of a reasonable internal structure for expansion shocks having pressure drops of over 2.5 atm. These computations also serve to verify the predictions of previous investigators. In particular, it appears that the local value of the entropy will attain a local minimum in the interior of expansion shocks; this contrasts sharply with the variation in compression shocks. The prediction that the Mach number no longer decreases monotonically has been verified; as predicted, the local Mach number has a maximum or minimum near the point where the local value of Γ changes sign. The prediction of a local minimum in the shock thickness with respect to strength is also verified. Evidence of this local minimum can be seen in figure 6 and tables 2 and 3. This local minimum is expected to occur when the sonic shock is the shock of maximum, rather than minimum, strength. In turn, the sonic limit is only possible when Γ changes sign; thus, the local minimum in thickness only occurs in cases of mixed nonlinearity. As discussed by Cramer (1987*a*), the physical effects leading to this phenomenon are the weakening of the local nonlinearity as the sonic condition is approached inside the shock layer rather than the well-known effects of viscosity variation.

A new phenomenon not anticipated in previous investigations is impending shock splitting. This phenomenon is expected to occur in compression shocks which take the flow from one side of the $\Gamma < 0$ region to the other. Both our numerical studies of the full equations and the extended weak-shock approximation developed in §5 indicate that impending shock splitting will always occur as the shock-splitting condition is approached. In the weak-shock approximation of §5 the inflexion points in the density distribution and the local maximum and minimum in the entropy distribution occur where the Rayleigh line is parallel to the shock adiabat (this is the Q-curve of figures 13 and 14). In terms of the (p, V)-diagram, admissible compression shocks which take the flow from one side of the $\Gamma < 0$ region to the other are expected to exhibit impending shock splitting if

$$\left.\frac{\mathrm{d}p}{\mathrm{d}V}\right|_{i'} < \frac{[p]}{[V]} < \left.\frac{[p]}{[V]}\right|_{\mathrm{ss}} < 0,$$

where $\mathrm{d}p/\mathrm{d}V$ denotes the slope of the shock adiabat, the subscript i' denotes the low-density zero of Γ and $([p]/[V])|_{\mathrm{ss}}$ denotes the slope of the Rayleigh line corresponding to shock splitting. Although this criterion was derived on the basis of the weak-shock approximation, it appears to give reasonable guidance for the exact problem.

A new feature which is also unique to impending shock splitting is the existence of an internal layer of supersonic flow. This again appeared in both numerical and analytical approaches.

Although the novel phenomena presented here are of interest in their own right, we feel these results can have a broader relevance. Perhaps the most important consideration is that many numerical schemes for inviscid flow have either numerical viscosity or deliberately incorporate artificial viscosity. To the extent that these viscosities mimic Navier–Stokes viscosity and heat conduction, such numerical

schemes will generate results similar to those presented here. For example, if a shock-capturing scheme is used to compute the supersonic flow of a BZT fluid, numerically generated impending shock splitting could be mistaken for inviscid splitting. Without the background provided here, it is at least conceivable that the non-monotone character of the Mach number or the negative entropy humps could also be misinterpreted. It should also be noted that the maximum-slope criterion for the shock thickness is no longer useful when impending shock splitting occurs; this is due to the appearance of additional inflexion points. A condition based on the percentage of the transition would be a better choice.

The seeds of the idea for the approximation of §5 were planted many years ago in conversations with Professor A. Kluwick. The first author would like to take this opportunity to acknowledge the many direct and indirect contributions of Professor Kluwick to this and related work.

REFERENCES

BETHE, H. A. 1942 The theory of shock waves for an arbitrary equation of state. *Office Sci. Res. & Dev. Rep.* 545.

CRAMER, M. S. 1987*a* Structure of weak shocks in fluids having embedded regions of negative nonlinearity. *Phys. Fluids* **30**, 3034–3044.

CRAMER, M. S. 1987*b* Dynamics of shock waves in certain dense gases. In *Proc. 16th Intl Symp. on Shock Tubes and Waves, Aachen, West Germany* (ed. H. Grönig), pp. 139–144. VCH.

CRAMER, M. S. 1989*a* Shock splitting in single-phase gases. *J. Fluid Mech.* **199**, 281–296.

CRAMER, M. S. 1989*b* Negative nonlinearity in selected fluorocarbons. *Phys. Fluids* A **1**, 1894–1897.

CRAMER, M. S. 1989*c* Nonclassical dynamics of classical gases. *Virginia Polytechnic Institute and State University Rep.* VPI-E-89-20.

CRAMER, M. S. & KLUWICK, A. 1984 On the propagation of waves exhibiting both positive and negative nonlinearity. *J. Fluid Mech.* **142**, 9–37.

CRAMER, M. S. & SEN, R. 1986 Shock formation in fluids having embedded regions of negative nonlinearity. *Phys. Fluids* **29**, 2181–2191.

CRAMER, M. S. & SEN, R. 1987 Exact solutions for sonic shocks in van der Waals gases. *Phys. Fluids* **30**, 377–385.

CRAMER, M. S. & SEN, R. 1990 Mixed nonlinearity and double shocks in superfluid helium. *J. Fluid Mech.* **221**, 233–261.

LAMBRAKIS, K. & THOMPSON, P. A. 1972 Existence of real fluids with a negative fundamental derivative Γ. *Phys. Fluids* **5**, 933–935.

LAX, P. D. 1971 Shock waves and entropy. In *Contributions to Nonlinear Functional Analysis* (ed. E. H. Zarantonello). Academic.

LEE-BAPTY, I. P. & CRIGHTON, D. G. 1987 Nonlinear wave motion governed by the modified Burgers' equation. *Phil. Trans. R. Soc. Lond.* A **323**, 173–209.

LIGHTHILL, M. J. 1956 Viscosity effects in sound waves of finite amplitude. In *Surveys in Mechanics* (ed. G. K. Batchelor & R. M. Davies), pp. 250–351. Cambridge University Press.

MARTIN, J. J. & HOU, Y. C. 1955 Development of an equation of state for gases. *AIChE J.* **1**, 142–151.

MENIKOFF, R. & PLOHR, B. 1989 Riemann problem for fluid flow of real materials. *Rev. Mod. Phys.* **61**, 75–130.

REID, R. C., PRAUSNITZ, J. M. & POLING, B. E. 1987 *The Properties of Gases and Liquids*, 4th edn. Wiley.

RIHANI, D. N. & DORAISWANY, L. K. 1965 Estimation of heat capacity of organic compounds from group contributions. *Ind. Engng Chem. Fundam.* **4**, 17–21.

TAYLOR, G. I. 1910 The conditions necessary for discontinuous motion in gases. *Proc. R. Soc. Lond.* A **84**, 371–377.

THOMPSON, P. A. 1971 A fundamental derivative in gasdynamics. *Phys. Fluids* **14**, 1843–1849.

THOMPSON, P. A. & LAMBRAKIS, K. 1973 Negative shock waves. *J. Fluid Mech.* **60**, 187–208.

ZEL'DOVICH, YA. B. 1946 On the possibility of rarefaction shock waves. *Zh. Eksp. Teor. Fiz.* **4**, 363–364.